Automotive Science and Engineering, Vol. 13, No. 2, (2023), 4092-4101

Iran University of Science and Technology

Automotive Science and Engineering

Journal Homepage: ase.iust.ac.ir

ISSN: 2008-9899

Simulation of Different Regimes of Biodiesel Spray's Wall Impingement on Combustion and Exhaust Gases of the Engine

Abbas Zarenezhad Ashkezari[1*], Reza Zirak[2]

[1]Associate Professor of Mechanical Engineering, Imam Khomeini Marine Sciences University, Nowshahr, Iran

[2]MSc of Mechanical Engineering, Islamic Azad University of Sari and Research and Self-Sufficiency Jihad of the IR Navy, Tehran, Iran

ARTICLE INFO

Article history:
Received: 18 Feb 2023
Accepted: 19 Mar 2023
Published: 15 Apr 2023

Keywords:
Spray
Wall impingement
Exhaust
Combustion
Biodiesel

A B S T R A C T

In the present study, different regimes of wall impingement in biodiesel spray were investigated in terms of emissions of diesel engines and performance and the best model for simulating the DI diesel engines fueled by biodiesel blends was presented. As shown by the findings, all aspects of wall impingement were considered in Walljet model, and it properly predicted the fuel droplet size generated by decomposition and penetration. Thus, it is possible to use it for simulating the biodiesel fuel spray atomization at varying engine operating conditions through the adjustment of the model constants.

1. Introduction

Wall film evolution and spray atomization can significantly affect pollution production and combustion efficiency. Liquid penetration in a DI diesel engine might be greater than the distance between the piston cavity wall and the nozzle tip, chiefly in engines with a low swirl or during cold starts. In this case, the spray-wall impingement can largely increase soot emissions and unburned hydrocarbon, particularly in the case of the formation of a wall film. Nevertheless, without the formation of a liquid wall film, it helps combustion under hot engine settings since vaporization and spray heating are intensified by drop breaking, leading to the large-scale gas vortex forming in the near-wall area. Consequently, for predicting the effects of the spray-wall impingement process on pollutant generation and engine performance in diesel, it is necessary to completely model these processes [1-2]. Considering the extensive use of DI diesel engines and the strict emission standards, it is required to examine spray-wall impingement approaches for understanding their impact on engine performance.

The experiment is mainly difficult to use to achieve information on spray-wall impingement. Consequently, it is possible to apply computational modeling in this case.

2. Impingement Regimes

A diesel spray impinging on a cylinder wall has a simultaneous or sequential collision with a group of droplets on a surface, and the impact of neighboring droplets is felt by each droplet collision. There are various factors that affect droplet behavior at wall interaction, such as diameter, droplet velocity, droplet properties, as well as liquid characteristics, including viscosity, surface tension, and temperature, and wall characteristics, including temperature and surface roughness, and wall film thickness.

*Corresponding Author
Email Address: azarenezhad.a@gmail.com
https://doi.org/10.22068/ase.2023.639

[DOI: 10.22068/ase.2023.639]

Fig. 1 shows different impingement regimes of a droplet-wall interaction. A droplet with little kinetic energy attaches to the wall in an unevenly spherical form, and its evaporation remains in the stick regime. When a droplet hits a wet or dry wall with moderate velocity, it results in its spreading and combining with the wall film (wet wall), or a wall film (dry wall) is formed. It is followed by reflection without breaking up in case of rebounding. When the walls are hot and dry, this regime happens. In this case, the contact between the wall and drop is hindered by a vapor cushion. Rebounding is observed with a wet wall when there is a modest impact energy and energy loss is minimized by an air layer between the liquid film and drop. Due to fast liquid boiling on a heated wall, the droplet is disintegrated in the boiling-induced break-up phase. The wall should have a temperature close to the Nakayama temperature (TN). It is the temperature at which the maximum evaporation rate of droplet is reached. In the hot surface, the droplet deformation into a radial film occurs that breaks because of thermo-induced instability in the case of a break-up. With extremely high impact energy, the splash regime is observed. It is followed by the formation of a crown and formation of jets on the crown's periphery, becoming unstable and being disintegrated into a large number of droplets [3].

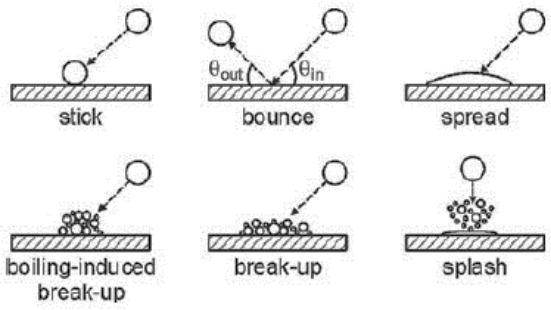

Figure 1: Various impact regimes [3]

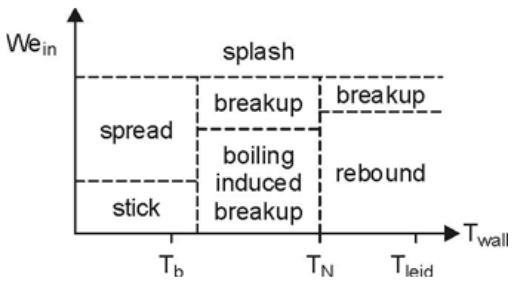

Figure 2: Droplet impingement regimes and transition conditions for a dry wall [3]

Use Two essential numbers exist concerning impingement regimes. The Weber number (We) that assesses the relative importance of surface tension and viscous forces working on the liquid (μ_d dynamic viscosity of liquid). The other number is the Laplace number that obtains the ratio of the kinetic energy (d: liquid density, u_n: velocity component normal to the surface, d_d: droplet diameter) and surface energy of the droplet. It is also possible to use the Ohnesorge number $Z = La^{-1/2}$ for representing the Laplace number.

$$We=\rho_d d_d u_n^2/\sigma \quad (1)$$

$$La=\rho_d \sigma\, d_d/\mu_d^2 \quad (2)$$

The other important factor affecting the impingement process is the wall temperature.

$$T_b<T_N<T_{leid} \quad (3)$$

Three distinctive temperatures in this process are as follows: The liquid boiling temperature Tb, the Nakayama temperature TN, where the maximum evaporation of droplet is reached, and the Leidenfrost temperature T_{leid}, where a thin layer of vapor is formed between the drop and surface and evaporation is minimized. Fig. 2 shows transition circumstances and droplet impingement regimes for a dry wall with a fixed Laplace number and surface roughness [4]. The wall has temperatures below the fuel's boiling point during injection in internal combustion engines [4]. It reduces the number of related impingement regimes with a dry wall sticking, spreading, and splashing. As found by Kolpakov et al. [5], with increasing the impact Weber number, it increases the sticking, rebounding, spreading, and splashing in regimes. A new spray/wall impingement model was developed by Ma et al. [6] based on droplet impact measurements. They studied the morphology dynamics of corona splash and prompt splash. Their findings indicated their success in the estimation of spray impingement. Du et al. [7] examined the injection pressure impact on the structure of the spray following wall impingement under the constant injection mass. Their results showed that with higher injection pressure, a higher vapor phase spray cone angle was obtained. Lee et al. [8] studied the spray behavior effects on particle number emissions. According to their findings, the in-cylinder flow considerably influences the sprays at higher injection pressures. They also found that higher pressure injection at late injection timing rises particle emissions. In the study by Wang et al. [9], the effects of wall and diesel spray interaction on ignition stability at

[DOI: 10.22068/ase.2023.639]

critical conditions at varying ambient temperatures with low ambient density were empirically examined. According to their findings, the increase in the ambient temperature reduced ignition delay time. Nevertheless, all ignition cases happened nearby the wall surface and away from the axis of the nozzle.

3. Biodiesel Fuel

Since the components of biodiesel fuels and MB have the same ester functional group, MB was used as a biodiesel fuel surrogate. The comparisons of viscosities, densities, surface tensions, as well as latent heat of vaporizations between MB (methyl butanoate) and diesel fuel are shown in Table 1 [10]. Surface tension and density of diesel are both below those of MB. Due to the larger MB viscosity at lower temperatures, similar viscosities are observed in both fuels with the temperature hitting 400 K. Two fuels have slightly different latent heat of vaporization. The increased initial spray momentum of MB leads to longer spray penetration and larger densities. Due to the importance of surface tension and viscosity variables for droplet breakdown, a larger liquid size and longer breakup length are required for MB spray.

Table 1: Various characteristics of diesel and biodiesel fuel [10]

Fuel properties	Diesel	Biodiesel (MB)
Density (g/cm^3)	0.840	0.898
Molar weight (g/mol)	100.2	102.1
Heat of vaporization (kJ/mol)	132.9	141.4
Cetane number	50.55	55.3
Boiling point (K)	372	376
Heat of combustion (kJ/mol)	2945.5	4849.2

4. Biodiesel Fuel

4.1. Walljet Model

This model is conceptually based on the spray-wall impingement model proposed by Naber and Reitz. Engine operation is simulated in the Walljet model: a vapor layer is created between the wall and droplet, and whether it falls back or slides on the wall is determined by the droplet Weber number [11].

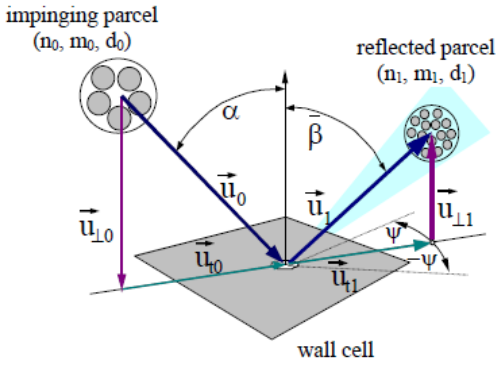

Figure 3: Wall Interaction of Droplets [11]

The critical Weber's number is 80. Although the previous figure shows a vertical velocity component in the wall's tangential component and can change with reducing the Weber number, the phenomenon back in less than this number drops rapidly. The following relation shows the experimental relationship between the droplet's Weber number and the Weber number of drops prior to dealing:

$$We_{norm,out} = C_1 . We_{norm,in} . e^{-C_2 We_{norm,in}} \quad (4)$$

0.687 and 0.04415 values were obtained as empirical constants C_1 and C_2. Consequently, the reflection angle changes in the range of 0-5 [12, 13]. It will be discovered what tangential angle on the surface is reflected in the shifting range of $-180<\psi<+180$. This angle is specified by a probability distribution function:

$$\psi = -\frac{\pi}{k} \ln\left[1-p\left(1-e^{-k}\right)\right] \quad (5)$$

In this situation, a random integer between 0 and 1 is created using the relation below, which may change the parameter k:

$$\sin\alpha = \left(\frac{e^k+1}{e^k-1}\right) \frac{1}{1+\left(\frac{\pi}{k}\right)^2} \quad (6)$$

After the alteration in droplet diameter, Weber numbers changes as:

$$\begin{cases} We<50 & d_1 = d_0 \\ 50 \le We \le 300 & d_1 = d_0 \ f(We_{norm,in}) \\ We>300 & d_1 = 0.2\ d_0 \end{cases} \quad (7)$$

4.2. Mundo Tropea Sommerfeld Model

[DOI: 10.22068/ase.2023.639]

This model is on the basis of the studies by Mundo, Tropea, and Sommerfeld [14]. These authors identified splash and deposition as the two regime types. The whole droplet is deposited on the wall in the deposition regime, while a part of the droplet is deposited in the splash regime and the remaining is reflected away from the wall. The splashing parameter K, is given as W1 in the list of the model parameters and this parameter can define the transition from one regime to the other.

$$K=W_1=\sqrt{We\sqrt{Re}}=Oh\,Re^{1.25} \tag{8}$$

The following relations are used to calculate Ohnesorge and Reynolds numbers:

$$Re=\frac{\rho_1 D_{pi} v_{ni}}{\mu_1} \tag{9}$$

$$Oh=\frac{v_{ni}}{\rho_1 \sigma D_{pi}} \tag{10}$$

K =W_1 =57.5 is independent of surface roughness, while when specifying the quantity of mass sprayed and the splashed droplets' diameter, different formulae are used for a rough and a smooth wall.

$$\text{smooth wall}\begin{cases}\frac{m_o}{m_i}=3.9896\times10^{-21}\times W_1^{9.2133}\\ \frac{d_o}{d_i}=0.88-0.013\times W_1 0.8\end{cases} \tag{11}$$

$$\text{rough wall}\begin{cases}\frac{m_o}{m_i}=8.035\times10^{-11}\times W_1^{4.1713}\\ \frac{d_o}{d_i}=0.43-0.0003\times W_1 0.9\end{cases}$$

The authors measured the following ratios of entry and exit tangential and normal velocities during the experiments:

$$\text{smooth wall}\begin{cases}\frac{v_{t_o}}{v_{t_i}}=1.068\\ \frac{v_{n_o}}{v_{n_i}}=0.208\end{cases} \tag{12}$$

$$\text{rough wall}\begin{cases}\frac{v_{t_o}}{v_{t_i}}=0.965\\ \frac{v_{n_o}}{v_{n_i}}=0.407\end{cases}$$

4.3. Bai and Gosman Model

This model considers splashing for values above the user-defined splashing parameter W_1. It is possible to use model parameters W_3 and W_4 for changing the roughness and smoothness, and the wet and dry conditions. The dry wall model presents two modes as splash and adhesion [15]. With the Weber number below Wet, the droplet is deposited on the wall, and the droplet splashes if it is greater. The following relation is used to calculate Wet:

$$We_C=A\times L\times\alpha^{-0.18} \tag{13}$$

where A represents a constant relying on the surface roughness. (rough, A = 1322) (smooth, A = 5264). There are three modes regarding a wet wall. With a Weber number W_2 below 5, the droplets rebound. After interaction, the droplet behaves as a solid particle with the following velocities:

$$v_{t_o}=\frac{5}{7}v_{n_i} \tag{14}$$

$$v_{n_o}=-e\times v_{n_i} \tag{15}$$

$$e=0.993-1.76\theta_i+1.56\theta_i^{\,2}-0.49\theta_i^{\,3} \tag{16}$$

The mass ratio of the entering and departing droplets is specified as in the splashing regime occurring above splashing parameter K>W_1 =57.5.

$$\begin{aligned}&\text{dry wall} && \frac{m_o}{m_i}=0.2+0.6R\\ &\text{wet wall} && \frac{m_o}{m_i}0.2+0.9R\end{aligned} \tag{17}$$

The total number of product droplets N formed by a splashing event is determined by this model rather than specifying the appropriate product droplet size.

$$N=a_0\left(\frac{We}{We_t}-1\right) \tag{18}$$

A value of 5 for the constant a_0 has been recommended by the references. As the next phase, two product packs are created. In the first parcel, the number of droplets is randomly selected from the droplets' total number, followed by the distribution of the remaining droplets to the second parcel. By momentum conservation and energy considerations, the absolute velocities u_1 and u_2 of the product droplets are specified [15].

4.4. O'Rourke and Amsden Model

[DOI: 10.22068/ase.2023.639]

A splash Mach number E [16] was calculated by these authors rather than using the dimensionless parameter K. The default value for model parameter W1 was set as of 57.5. With the model parameter W2 as 1, it is possible to use this model together with the wall film model. A fixed average wall film thickness with model parameter W3 for W2 equal to zero can be prescribed to approximate wet conditions. Model parameter W4 specifies the transition film thickness between dry and wet conditions. The Mach number stays the same for the splash.

$$E^2 = \frac{\rho_1 D_{p_i} v_{n_i}}{\sigma} \frac{1}{\min\left(\frac{h_0}{D_{p_i}},1\right)+\frac{\delta_{b_1}}{D_{p_i}}} \quad (19)$$

where b_l denotes the boundary layer's thickness, and h_0 represents the thickness of the film.

$$\delta_{b_1} = \frac{D_{p_i}}{\sqrt{Re}} \quad (20)$$

E denotes equivalent to the splash prerequisite for a dry wall with h_0 as 0. With dissipation of the energy for viscous damping, it inhibits the droplets splashing with thickening the wall film. The following relation defines the ratio of entering mass to departing mass:

$$\frac{m_o}{m_i} = \min\left(18\times10^{-4}\left(E^2-E_c^{\,2}\right)0.75\right) \quad (21)$$

The size of the outgoing droplets is sampled using a Nukiyama-Tanasawa distribution. Also, using Nukiyama-Tanasawa distributions, the outgoing tangential and normal velocities of droplets are sampled. The final tangential droplet direction as in the Naber Reitz model is calculated using the same process.

5. Modeling and Numerical Method

3D modeling of the combustion chamber of a diesel engine was used to design engine cylinder in SolidWorks. With the piston at TDC, based on the approach used to create a mesh in AVL FIRE software, it is required to have a surface mesh of the model generated by ANSYS ICEM CFD software. At this phase, the AVL FIRE software is used on the surface mesh. Then, engine geometry is three-dimensionally modeled and the moving mesh is created. The boundary surfaces with the appropriate names are selected to apply boundary conditions at this point. The areas on the final mesh in the engine are depicted in Fig. 4.

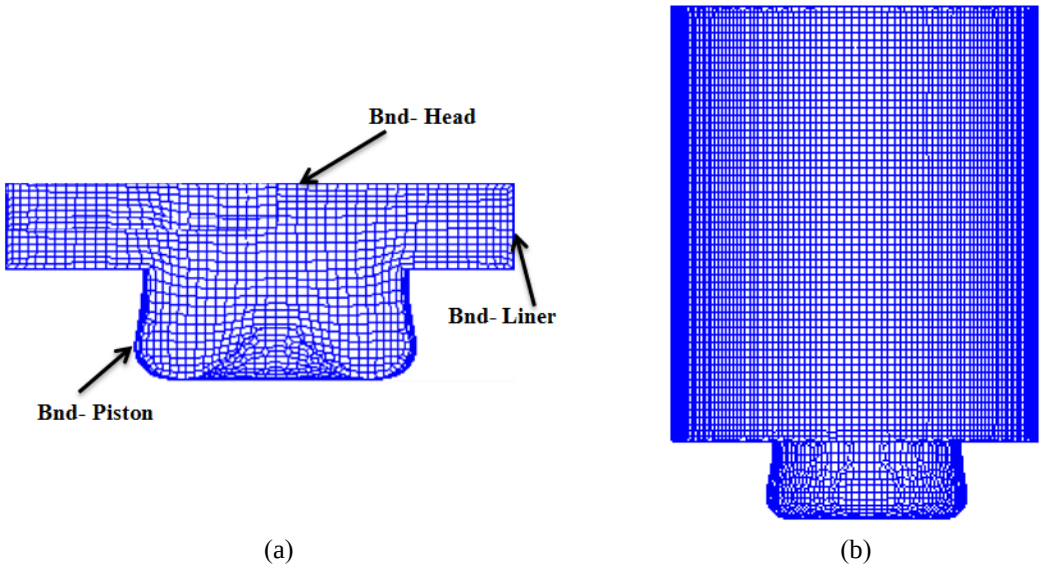

(a) (b)

Figure 4: (a) Computational grid with boundary conditions, (b) Final computational grid at BDC

Diesel engine combustion was simulated using AVL FIRE based on a finite volume approach. To this end, a biodiesel blend (20% MB was used as a biodiesel fuel + 80% pure diesel fuel) through discretizing the ruling equations of momentum, mass, and energy continuity with the turbulence model. An iterative process is then used to solve the obtained algebraic equations. The Shell model for ignition [17]. The ECFM-3Z model based on the Coherent flame model was used for biodiesel combustion modeling [18, 19], the Standard k-model for turbulence [20], the Dukowicz model for heat transfer and evaporation of fuel droplets [21, 22], the extended Zeldovich mechanism for NO_x

[DOI: 10.22068/ase.2023.639]

emission [23], and the Hiroyasu mechanism for soot formation [24, 25] were all utilized in the present work. The engine specifications are given in Table 2.

Table 2: Engine specifications

Engine type	One cylinder DI diesel engine
Bore × Stroke	125 mm × 140 mm
Compression ratio	16:1
Displacement	1.72 Lit
IVC	153° CA bTDC
EVO	116° CA aTDC
Number of orifices	6
Engine speed	800 rpm
Start of injection	16° CA bTDC
Initial pressure	240 kPa
Initial temperature	301 K

6. Results and Discussion

It is required to evaluate the computational mesh for independence from the solution for ensuring the quality of calculations and accuracy of simulation results. For re-stimulating the engine combustion chamber shape, the authors used 67229 and 73075 cells, which had been simulated by 61383 cells in TDC. The cell numbers in TDC for each of the three modalities are shown in Table 3. By making a comparison among the in-cylinder pressure curves, a negligible difference was found in peak pressure between modes 2 and 3, while it is a significant difference between modes 1 and 2. The computational mesh with 67229 cells in TDC was selected as the proper computational mesh given the results achieved by considering the situation and value of in-cylinder peak pressure and the computation time. Considering trivial changes between the results in the 0.25, 0.5, and 1-degree time steps, the 1° CA time step with 67229 cells in TDC was selected as the principal model for reducing calculation time.

Table 3: Grid dependence study

Computational Mesh	Cells at TDC	In-cylinder Peak Pressure
1	61383	7.48 (MPa)
2	67229	6.92 (MPa)
3	73075	6.97 (MPa)

6.1. Validation

The present study examined four models with different fuel spray wall-impingements for investigating the biodiesel spray wall-impingement model's impact on the emissions and combustion in a DI diesel engine. The in-cylinder pressure with Walljet model are shown in Fig. 5. The empirical data utilized for validating the numerical results were presented by Cheng et al. [26]. After correctly calculating the ignition timing, the predicted in-cylinder pressure showed an acceptable consistency with the empirical data.

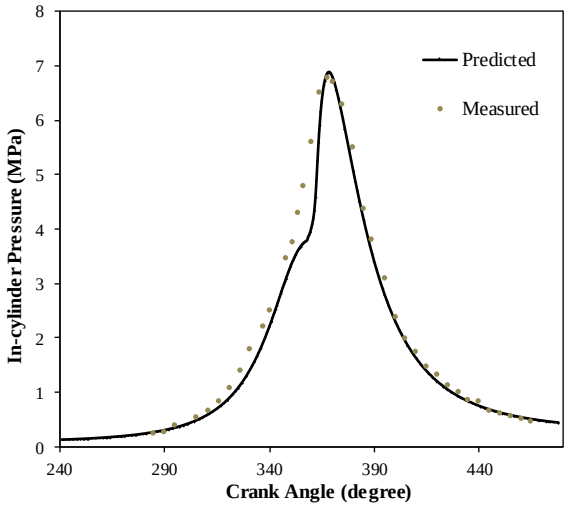

Figure 5: Comparison of measured and predicted in-cylinder pressure, Initial pressure = 0.2 MPa, Initial temperature = 301 K, and speed = 800 rpm [26]

Compared to the empirical diagram [26], the in-cylinder pressure vs. crank angle for different models of biodiesel spray wall-impingement (with the engine utilizing 20% biodiesel fuel) is displayed in Fig. 6. It is observed that all four models properly forecast the qualitative behavior of in-cylinder pressure changes. However, the closest match to the empirical result is provided by

[DOI: 10.22068/ase.2023.639]

the Walljet model, principally concerning in-cylinder peak pressure and its location.

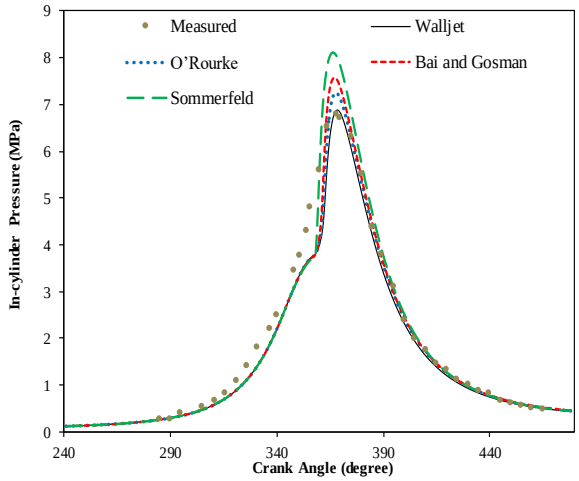

Figure 6: Predicted in-cylinder pressure for several models of biodiesel spray wall impingement, Initial pressure = 0.2 MPa, Initial temperature = 301 K, and speed = 800 rpm

Figures 7 and 8 show the in-cylinder temperature and heat release rate for different spray wall-impingement models. NOx and soot emissions are compared for different models in Figures 9 and 10. In comparison with other models, the Walljet model showed lower peak temperature and premixed peak pressure, with the maximum amount of soot and the lowest NO_x pollutant. On the other hand, the Sommerfeld model showed a totally distinct behavior pattern.

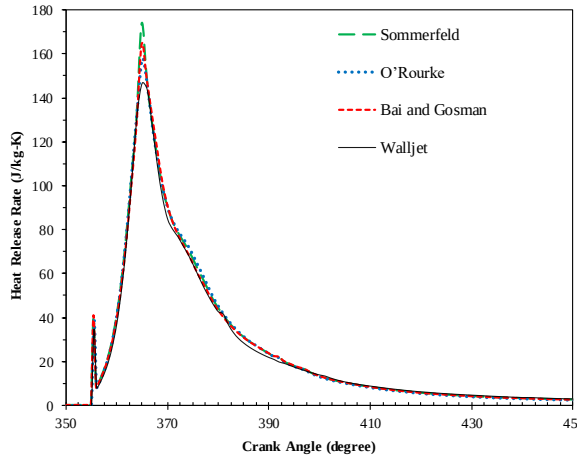

Figure 7: The heat release rate for various biodiesel spray wall-impingement models, Initial pressure = 0.2 MPa, Initial temperature = 301 K, and speed = 800 rpm

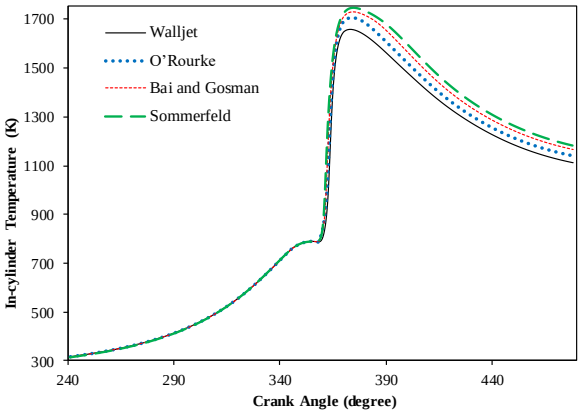

Figure 8: In-cylinder temperature for various biodiesel spray wall-impingement models, Initial pressure = 0.2 MPa, Initial temperature = 301 K, and speed = 800 rpm

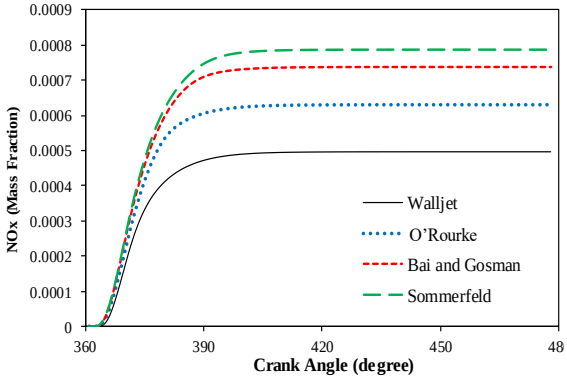

Figure 9: NO_x emission changes in various biodiesel spray-wall impingement models

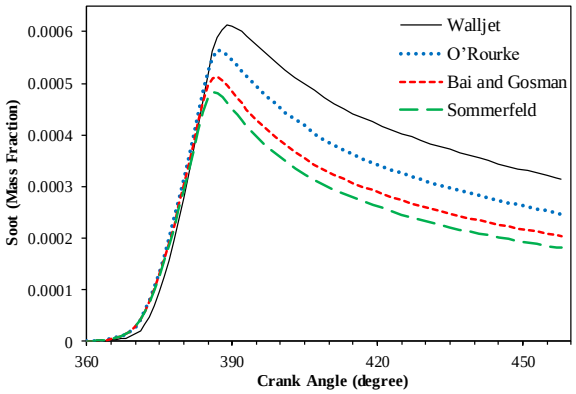

Figure 10: Soot emission changes in various biodiesel spray-wall impingement models

The interaction between spray droplet and streamline flow at 5 aTDC is shown in Fig. 11 for different spray-wall impingement models. It is observed that as a result of the evolution of the

[DOI: 10.22068/ase.2023.639]

piston bowl and cylinder, the spray droplet distributes from the central line. Better combustion and fuel-air mixing is obtained in the Walljet model with more evenly distributed spray droplets. The preceding data show less precision in forecasting spray drop mass and drop sizes in the models proposed by Sommerfeld and Bai and Gosman models. Additionally, the precision of predicting the spray post-impingement characteristics (e.g., the fraction of mass deposited on the wall, rebound velocity, velocity and size distributions of secondary droplets) for the splash regime by O'Rourke model is less than the Walljet model.

The Walljet model enhanced evaporation along with decreasing the amount of remaining fuel, inferring a quicker disintegration and splash of large droplets.

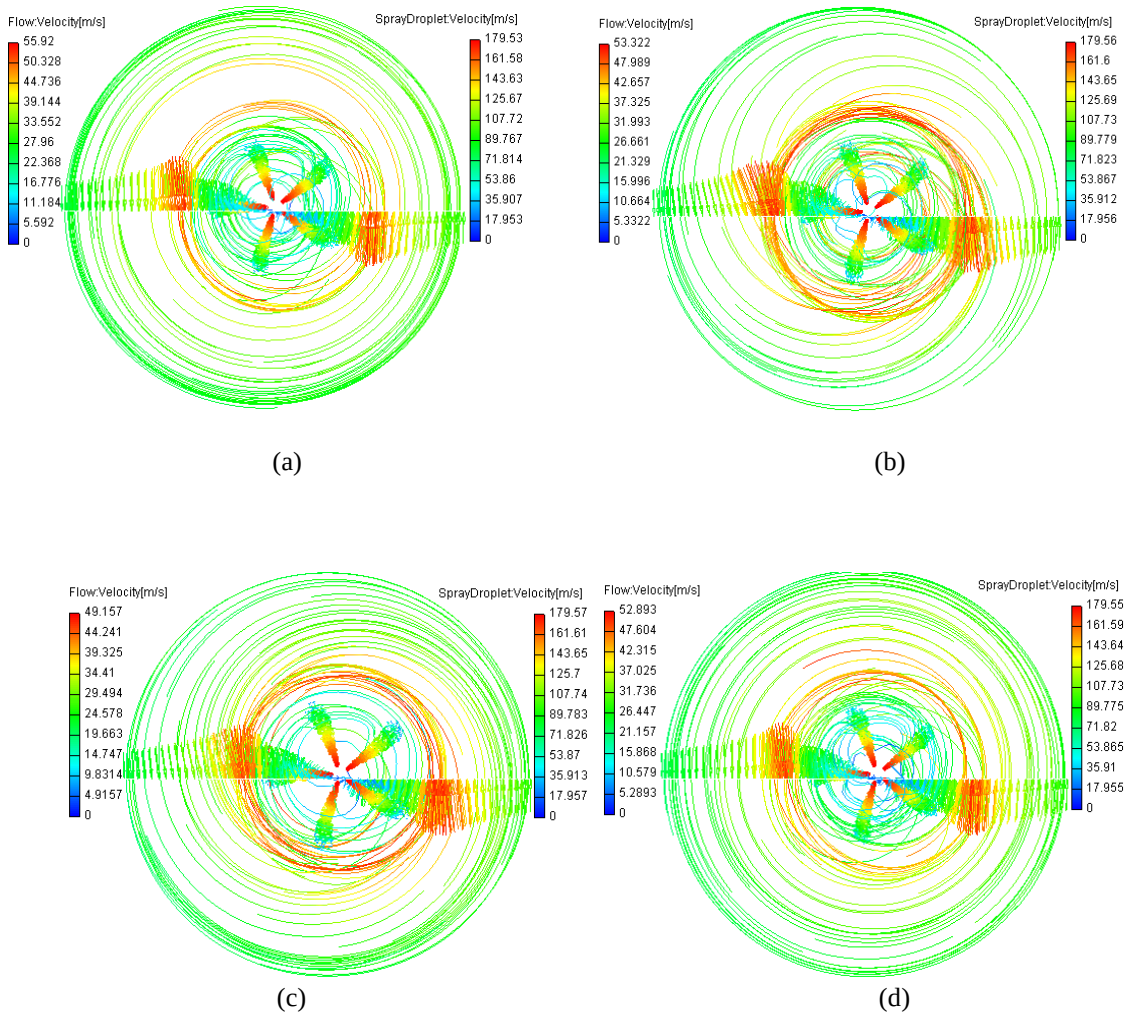

Figure 11: Interaction between streamline flow and spray droplet at 5 aTDC for difference models, (a) Sommerfeld, (b) Bai and Gosman, (c) O'Rourke, (d) Walljet

[DOI: 10.22068/ase.2023.639]

7. Conclusions

A Different spray-wall impingement models were used in the present work for simulating the biodiesel spray-wall interaction, and we investigated the impact of these models on DI diesel engine combustion and spray characteristics. In order to run the DI diesel engine on biodiesel, we validated and compared the results with the empirical data. An acceptable agreement between empirical and anticipated results ensured the precision of the numerical predictions obtained in this work. The investigation of biodiesel engine spray-wall impingement by the utilization of four models presented the following results:

- It is crucial to understand the fuel spray-wall impingement mechanism in order to provide an accurate simulation of the following mixture formation processes, and pollutant generation and combustion.
- All fuel spray-wall impingement models present an accurate capturing of the peak pressures and ignition timing.
- In comparison with the estimations from other models, the Sommerfeld model presented a better prediction of drop mass and sizes.
- A quicker decomposition and splash of large drops is provided by the Walljet model. It also presents a lower amount of leftover fuel and higher evaporation, which provides a better fit to empirical data.

Declaration of Conflicting Interests

The authors declared no potential conflicts of interest with respect to the research, authorship, and/or publication of this article.

References

[1] A. Zarenezhad Ashkezari, A. Hossein Nezhad, S. Farahat, Reduction of pollutant emissions by developing a vaiable valve timing system in a direct injection diesel engine using computaional fluid dynamics modeling, Environmental Proggress and Sustainable Energy, Vol.35, (2016), pp.1430-1440.

[2] A. Zarenezhad Ashkezari, K. Divsalar, R. Malmir, I. Abbaspour, Emission and performance analysis of DI diesel engines fueled by biodiesel blends via CFD simulation of spray combustion and different spray breakup models: a numerical study. Journal of Thermal Analysis and Calorimetry, Vol.139, No.4, (2020), pp.2527-2539.

[3] C. Baumgarten, Mixture Formation in Internal Combustion Engine, New York: Springer-Verlag Berlin Heidelberg,(2006)..

[4] C. Chevalier, J. Warnatz, H. Melenk, Automatic generation of reaction mechanisms for the description of the oxidation in higher hydrocarbons. Berichte der Bunsen-Gesellschaft für Physikalische Chemie Vol.94, (1990).

[5] S. Pöttker, P. Eckert, T. Delebinski, C. Baumgarten, K. Oehlert, G. P. Merker, U. Wagner, U. Spicher, Investigations of HCCI combustion using multi-stage direct- injection with synthetic fuels. SAE paper (2004), 01–2946.

[6] T. Ma, L. Feng, H. Wang, H. Liu, M. Yao, A numerical study of spray/wall impingement based on droplet impact phenomenon. International Journal of Heat and Mass Transfer. Vol.112, (2017), pp.401–412.

[7] W. Du, O. Zhang, W. Bao, J. Lou, Effects of injection pressure on spray structure after wall impingement. Applied Thermal Engineering, Vol.129 (2018), pp.1212–1218.

[8] Z. Lee, D. Kim, S. Park, Effects of spray behavior and wall impingement on particulate matter emissions in a direct injection spark ignition engine equipped with a high pressure injection system. Energy Conversion and Management, Vol.213, (2020), 112865.

[9] D. Wang, Z. Shi, Z. Yang, H. Chen, M. Wang, Y. Li, Experimental study of wall-impinging diesel spray ignition and combustion

[DOI: 10.22068/ase.2023.639]

characteristics under critical conditions, Fuel, Vol.15, (2022), 121976.

[10] C. L. Yaws, Chemical properties handbook: physical, thermodynamic, environmental, transport, safety, and health related properties for organic and inorganic chemicals. New York: McGraw-Hill, (1999).

[11] J. D. Naber, R. D. Reitz, Modeling engine spray/wall impingement. SAE, (1988), 880107.

[12] C. Mundo, M. Sommerfeld, C. Tropea, Droplet-wall collisions: experimental studies of the deformation and breakup process, International Journal of Multiphase Flow, Vol.21, No.2, (1995), pp.151–173.

[13] C. Mundo, M. Sommerfeld, C. Tropea, Experimental studies of the deposition and splashing of small liquid droplets impinging on a flat surface.in: A J Yule, C. Dumouchel (Eds.), Proceedings of the 6th International Conference of Liquid Atomization Spray System, Rouen, France, (1994), pp.134–141.

[14] C. Mundo, M. Sommerfeld, C. Tropea, Deposition and splashing of small liquid droplets impinging on a flat surface, ICLASS, Rouen, France, (1994).

[15] C. Bai, A. D. Gosman, Development of methodology for spray impingement simulation. SAE Paper (1995), 950283.

[16] P. J. O'Rourke, A. A. Amsden, A spray/wall interaction submodel for the KIVA-3 wall film model. SAE Paper, (2000), 01-0271.

[17] M. Halstead, L. Kirsch, C. Quinin, The auto ignition of hydrocarbon fueled at high temperatures and pressures–fitting of a mathematical model. Combustion Flame, Vol.30, (1977), pp.45-60.

[18] O. Colin, A. Benkenida, C. Quinn, The 3-zones extended coherent flame model (ECFM3Z) for computing premixed/diffusion combustion, Oil & Gas Science and Technology, Vol.59, (2004), pp.593-609.

[19] J. Helie, A. Trouve, C. Quinn, A modified coherent flame model to describe turbulent flame propagation in mixtures with variable composition, Proceedings of the Combustion Institute, Vol.28, (2000), pp.193-201.

[20] V. Yakhot, S. A. Orszag, S. Thangam, T. B. Gatski, C. G. Speziale, Development of turbulence models for shear flows by a double expansion technique, Physics of Fluids, Vol.4, (1992), pp.139-158.

[21] J. K. Dukowicz, A particle-fluid numerical model for liquid sprays, Journal of Computational Physics, Vol.35, (1980), pp.229-253.

[22] D. Mewes, F. Mayinger, Heat and mass transfer, Germany:Springer-Verlag Berlin Heidelberg GmbH. (2008).

[23] G. A. Lavoie, J. B. Heywood, J. C. Keck, Experimental and theoretical study of nitric oxide formation in internal combustion engines. Combustion Science Technology, Vol.1, (1970), pp. 313–326.

[24] H. Hioyasu, K. Nishida, Simplified three dimensional modeling of mixture formation and combustion in a DI diesel engine, SAE (1989), 890269.

[25] J. Nagle, R. F. Strickland-Constable, Oxidation of carbon between 1000-2000 C, Proceedings of the Fifth Conference on Carbon, New York: Pergamon, (1962).

[26] A. S. Cheng, A. Upatnieks, C. J. Mueller, Investigation of the impact of biodiesel fuelling on NO_x emissions using an optical direct injection diesel engine, International Journal of Engine Research, Vol.7, No.4, (2006), pp.297-318.

[DOI: 10.22068/ase.2023.639]